Relativistic Hydrodynamic Evolutions with Black Hole Excision

Matthew D. Duez[1], Stuart L. Shapiro[1,2], and Hwei-Jang Yo[1,3]
[1] *Department of Physics, University of Illinois at Urbana-Champaign, Urbana, IL 61801*
[2] *Department of Astronomy, & NCSA, University of Illinois at Urbana-Champaign, Urbana, IL 61801*
[3] *Institute of Astronomy and Astrophysics, Academia Sinica, Taipei 115, Taiwan, Republic of China*

We present a numerical code designed to study astrophysical phenomena involving dynamical spacetimes containing black holes in the presence of relativistic hydrodynamic matter. We present evolutions of the collapse of a fluid star from the onset of collapse to the settling of the resulting black hole to a final stationary state. In order to evolve stably after the black hole forms, we excise a region inside the hole before a singularity is encountered. This excision region is introduced after the appearance of an apparent horizon, but while a significant amount of matter remains outside the hole. We test our code by evolving accurately a vacuum Schwarzschild black hole, a relativistic Bondi accretion flow onto a black hole, Oppenheimer-Snyder dust collapse, and the collapse of nonrotating and rotating stars. These systems are tracked reliably for hundreds of M following excision, where M is the mass of the black hole. We perform these tests both in axisymmetry and in full 3+1 dimensions. We then apply our code to study the effect of the stellar spin parameter J/M^2 on the final outcome of gravitational collapse of rapidly rotating $n = 1$ polytropes. We find that a black hole forms only if $J/M^2 < 1$, in agreement with previous simulations. When $J/M^2 > 1$, the collapsing star forms a torus which fragments into nonaxisymmetric clumps, capable of generating appreciable "splash" gravitational radiation.

PACS numbers: PACS numbers: 04.25.Dm, 04.70.-s, 04.30.Db

I. INTRODUCTION

Since many of the most interesting phenomena in astrophysics involve black holes, the modeling of black hole spacetimes is one the most important problems in numerical general relativity. It is also one of the most challenging problems. Black hole evolutions present all the usual difficulties of numerical relativity, such as the need to find a stable form of the field evolution equations and the need to find a practical coordinate system. In addition, handling the singular region is very subtle for a numerical code; the black hole singularity must be avoided to allow the exterior evolution to continue far into the future.

One of the most promising methods to date of dealing with black hole singularities is black hole excision. This method, first suggested by Unruh [1], exploits the fact that the singularity resides inside an event horizon, a region that is casually disconnected from the rest of the universe. Since no physical information propagates from inside the event horizon to outside, one should be able to evolve the exterior independent of the interior spacetime. Inside the event horizon, causality entitles us to do anything which will produce a stable exterior evolution. In particular, one can excise a region inside the horizon containing the singularity and replace it with suitable boundary conditions at its outer surface.

Although it is guaranteed that no physical signal can propagate from inside the horizon to outside, unphysical signals often can propagate in evolution codes. Gauge modes can move acausally for many gauge conditions. Although they carry no physical content, such modes may destabilize the code. Thus, the choice of gauge is crucial to obtaining good excision evolutions. In addition, constraint-violating modes can, for some formulations of the field equations, propagate acausally, creating inaccuracies and instabilities. Thus, the choice of formulation is also crucial to obtaining good excision evolutions.

The feasibility of black hole excision was demonstrated in spherically symmetric 1+1 dimensional evolutions of a single black hole in the presence of a self-gravitating scalar field [2, 3, 4, 5]. Excision was also implemented successfully to study the spherically symmetric collapse of collisionless matter to a black hole in Brans-Dicke theory [6]. Three-dimensional evolutions of black holes with excision were attempted by using the standard 3+1 ADM formulation, for a stationary [7] and for a boosted black hole [8]. Although the introduction of excision improved the behavior of these black hole simulations, long-term stability could not be achieved due to instabilities endemic to the unmodified ADM formulation.

Since then, new and more stable formulations of the 3+1 Einstein field equations have been devised. Using excision in a modified version of the ADM equations commonly referred to as BSSN [9, 10], several groups have evolved stationary black hole spacetimes (non-spinning and spinning) for arbitrarily long times [11, 12]. Long-term stability has also been achieved using hyperbolic formulations of the field equations [13, 14, 15] and using characteristic evolutions [16]. Success has also been achieved in evolving distorted and moving black holes with excision, both with characteristic formalisms [16] and with BSSN [17, 18, 19]. Excision has also been used to simulate the grazing collision of two black holes [20] and to simulate binary black holes for approximately one orbital period [21].

The last several years also have seen significant advances in numerical, 3+1 relativistic hydrodynamics in

dynamical spacetimes (see, e.g. [22, 23, 24]). The simulation of rapidly rotating, relativistic stars is now possible, and fully relativistic evolution codes are being used to study the stability [25, 26] and gravitational collapse [27, 28, 29] of such objects. Binary neutron stars can now be evolved accurately for multiple orbits [24, 30], and numerical simulations have been used to study the final merger of these binaries [31, 32].

The necessary tools are clearly being forged to enable numerical relativity to model a wide variety of strong-field gravitational phenomena. Many interesting systems in astrophysics involve the simultaneous presence of both black holes and hydrodynamic matter fields, and these systems will require a code which can handle both in order to model them reliably.

One important scenario involving both hydrodynamic matter and black holes is core collapse in massive stars, an event of immense importance due to its association with supernovae, the formulation of neutron stars and black holes, and gamma ray bursts (GRBs). Some recent numerical simulations suggest [33] that a star must have mass less than about 20 $M_\odot$ for core collapse to result in a conventional neutron star and supernova explosion. For progenitor masses between around $20M_\odot$ and $40M_\odot$, the core collapses to a neutron star initially, but it eventually implodes to a black hole, as ejected material slowly falls back onto the remnant (see also [34]). For more massive stars, the core collapses promptly to a black hole. Such a massive system is a promising candidate for a GRB [35]. There is growing evidence that long duration GRBs are associated with hypernovae that accompany the collapse of massive stellar cores. This evidence includes the association of the low-energy GRB980425 with a supernova [36], the presence of supernova-like features in the optical afterglow of several GRBs [37], and the existence of freshly synthesized elements in the ejecta of GRB 011211 [38]. Most recently, a hypernova was found to be temporally and spatially coincident with a normal cosmological burst source, GRB 030329 [39]. Most models of the central engine of GRBs involve a black hole surrounded by a rapidly accreting disk and a jet [40]. Three dimensional fully relativistic simulations of both the black hole and the exterior matter will be needed to test the feasibility of various models for the production of GRBs from such "collapsars", and it is likely that excision will be required to track the full evolution.

The merger of binary neutron stars is a promising source of gravitational waves, as well as a prime candidate for short duration GRBs [41]. Binary mergers of stars of high compaction collapse promptly to a black hole [31]. The coalescence of low-compaction neutron stars probably leads to the formation of a hypermassive neutron star remnant [26, 32, 42] followed by a delayed collapse [43, 44]. Either way, excision of the black hole singularities is necessary to follow binary mergers which form black holes with accretion disks, emit gravitational waves, and drive short-duration GRBs.

The dynamics of accretion flows onto a black hole is another problem of great importance, since black holes are usually visible electromagnetically only through accretion. When the mass of the accreting fluid is much less than that of the black hole, then the matter can be evolved on a fixed black hole spacetime. When the masses of the hole and the matter are comparable, then a fixed black hole spacetime becomes a bad approximation to the true metric, and the full system must be evolved self-consistently. This is particularly important for determining if and when the disk may produce an instability, as in the runaway instability [45], or in the one-armed spiral instability [46] which can generate quasi-periodic gravitational waves [47].

Other coupled black hole-hydrodynamic matter systems include a neutron-star black hole binary, which might be an important source of gravitational radiation for LIGO, and also the disruption or capture of a star by a massive black hole, which is expected to be a major source of waves for LISA [48]. Supermassive black hole seed formation by the collapse of a massive or supermassive star is another important example [47, 49].

Successful attempts at evolving matter and a black hole together in a dynamical spacetime using excision have been rare. Scheel *et al.* [6] simulated the collapse of a spherically symmetric configuration of collisionless matter in Brans-Dicke theory with excision. The spacetime within the numerical domain was evolved until the appearance of an apparent horizon. At that time, an excision boundary was introduced and the evolution of the exterior spacetime was continued. An attempt to evolve a dynamical black hole spacetime with hydrodynamic matter was undertaken by Brandt *et al* [50] in axisymmetry. In that paper, a black hole is evolved with an accretion flow, using the ADM formalism and an isometry inner boundary condition at the apparent horizon. They were able to evolve several systems for up to about $100M$. Little progress has been made since then, presumably because the computational tools for performing excision and relativistic hydrodynamics in 3+1 had to be perfected independently. We have only now reached the stage where these tools can be put together successfully.

In this paper, we perform the first simulations which utilize excision to evolve relativistic hydrodynamic matter in 3+1 dynamical spacetimes containing black holes. In particular, we present evolutions of the gravitational collapse of stars from the beginning of collapse, through black hole formation, to quiescent final states. We perform these evolutions in two stages. From the beginning of collapse until the appearance of an apparent horizon, we evolve using our new, relativistic hydrodynamics (BSSN) code without excision (i.e. our "pre-excision" code). After an apparent horizon appears, we continue the evolution with a region inside the horizon excised. At the moment we introduce excision, a significant amount of matter is still outside the excision zone and the black hole is significantly distorted and in a nonstationary state. We follow its evolution to a final stationary state. In Section II we describe our evolution scheme, including

our gauge and boundary conditions. In Section III we describe our code diagnostics. In Section IV we test our code on systems with known behavior, including vacuum black holes, relativistic Bondi accretion, Oppenheimer-Snyder collapse, and the collapse of unstable polytropes, both non-rotating and rotating. We find that we are able to evolve many systems stably for hundreds of M. When we evolve systems with appreciable angular momentum, we can only conserve J for somewhat shorter durations, but this duration can be extended by increasing resolution. In Section V we apply our code to study the late-time outcome of pressure-depletion-induced gravitational collapse of rapidly-rotating polytropes with polytropic index $n = 1$. We find that stars with $J/M^2 < 1$ collapse to Kerr black holes with no surrounding disks. Stars with $J/M^2 > 1$ collapse to tori, which then fragment. This fragmentation process can produce copious amounts of gravitational radiation, originally referred to as "splash radiation" [51]. Finally, we summarize our results and discuss future improvements to our code in Section VI.

Throughout this paper, Latin and Greek indices denote spatial components (1-3) and spacetime components (0-3), respectively. We use geometrized units, so that $G = c = 1$.

II. SUMMARY OF METHOD

Our basic code has been described in detail in previous papers [12, 24] and will be discussed here only briefly to point out recent improvements. Our code evolves the full Einstein field equations coupled to relativistic hydrodynamics in 3+1 dimensions. We have recently generalized this code using the Cartoon methods of [27, 52] so that it can perform 2+1 simulations in axisymmetry in the same coordinate system. In order to improve its behavior near the intersection of the excision zone and the symmetry axis, we add a small amount of Kreiss-Oliger dissipation [53, 54, 55] to the evolution equation for the extrinsic curvature $\tilde{A}_{ij}$. A further description of our axisymmetry algorithms, together with axisymmetry code tests, will be presented in a forthcoming paper [44], in which the effects of viscosity on differentially rotating binary neutron star remnants are studied.

We evolve the field evolution equations using the BSSN formulation [9, 10]. In the BSSN system, one decomposes the 3-metric as $\gamma_{ij} = e^{4\phi}\tilde{\gamma}_{ij}$ and the extrinsic curvature as $K_{ij} = e^{4\phi}(\tilde{A}_{ij} + \tilde{\gamma}_{ij}K/3)$, and one promotes the conformal connection coefficients $\tilde{\Gamma}^i = -\tilde{\gamma}^{ij}{}_{,j}$ to independent variables. One then uses the ADM equations to write evolution equations for the new set of fundamental variables: $\tilde{\gamma}_{ij}$, ϕ, $\tilde{A}_{ij}$, K, and $\tilde{\Gamma}^i$. On each time slice, these variables must satisfy the following constraint equations:

$$0 = \mathcal{H} \equiv \tilde{\gamma}^{ij}\tilde{D}_i\tilde{D}_j e^{\phi} - \frac{e^{\phi}}{8}\tilde{R} + \frac{e^{5\phi}}{8}\tilde{A}_{ij}\tilde{A}^{ij} - \frac{e^{5\phi}}{12}K^2 + 2\pi e^{5\phi}\rho, \quad (1)$$

$$0 = \mathcal{M}^i \equiv \tilde{D}_j(e^{6\phi}\tilde{A}^{ji}) - \frac{2}{3}e^{6\phi}\tilde{D}^i K - 8\pi e^{6\phi}S^i \quad (2)$$

$$0 = \mathcal{G}^i \equiv \tilde{\Gamma}^i + \tilde{\gamma}^{ij}{}_{,j} \quad (3)$$

$$0 = \mathcal{D} \equiv \det(\tilde{\gamma}_{ij}) - 1 \quad (4)$$

$$0 = \mathcal{T} \equiv \mathrm{tr}(\tilde{A}_{ij}) \ . \quad (5)$$

These constraints are solved only at the initial time, and are used henceforward as diagnostics. In an attempt to improve the stability and accuracy of the BSSN formulation, one can add multiples of the above constraints to the field equations. Many possible modifications of this kind have recently been suggested [12, 56, 57, 58, 59, 60]. We found a slight improvement in ADM mass conservation by adopting the following modifications:

$$\partial_t\phi = \cdots + c_{H1}\Delta T\alpha\mathcal{H} \quad (6)$$

$$\partial_t\tilde{\gamma}_{ij} = \cdots + c_{H2}\Delta T\alpha\tilde{\gamma}_{ij}\mathcal{H} \quad (7)$$

$$\partial_t\tilde{A}_{ij} = \cdots - c_{H3}\Delta T\alpha\tilde{A}_{ij}\mathcal{H} \ , \quad (8)$$

where ΔT is the timestep, $c_{H1} = 0.1$, $c_{H2} = 0.5$, and $c_{H3} = 1$. [For the complete right hand sides of Eqs. (6)-(8), see [24], equations (12), (11), and (14).] Modifications similar to those in Eqs. (6) and (7) were suggested in [60], while a modification similar to Eq. (8) has recently been used in [61] for doing excision in the ADM formulation for pure vacuum spacetimes. Eq. (6) introduces a diffusive term into the evolution of ϕ. Eq. (8) introduces a nonlinear damping term into the evolution of $\tilde{A}_{ij}$. We find that modification (8) has the largest impact on accuracy.

Of crucial importance for the stability of our code are our constraint additions to the $\tilde{\Gamma}^i$ evolution equation. As shown in [24], our equation for $\partial_t\tilde{\Gamma}^i$ has the terms

$$\partial_t\tilde{\Gamma}^i = \frac{2}{3}\tilde{\Gamma}^i\beta^j{}_{,j} - \tilde{\Gamma}^j\beta^i{}_{,j} + \cdots \quad (9)$$

Looking, for example, at the x-component of this equation,

$$\partial_t\tilde{\Gamma}^x = \frac{2}{3}\tilde{\Gamma}^x\beta^j{}_{,j} - \tilde{\Gamma}^x\beta^x{}_{,x} - \cdots \quad (10)$$

we see that if $\beta^j{}_{,j} > 0$ or $\beta^x{}_{,x} < 0$, then $\partial_t\tilde{\Gamma}^x$ contains a term tending to produce exponential growth. We lessen the possibility of an instability caused by these terms by using (3) to replace (10) with

$$\partial_t\tilde{\Gamma}^x = \frac{2}{3}\left[\beta^j{}_{,j} + \lambda_A\left|\beta^j{}_{,j}\right|\right](-\tilde{\gamma}^{xk}{}_{,k}) - \frac{2}{3}\lambda_A\left|\beta^j{}_{,j}\right|\tilde{\Gamma}^x - \left[\beta^x{}_{,x} + \lambda_B\left|\beta^x{}_{,x}\right|\right](-\tilde{\gamma}^{xk}{}_{,k}) - \lambda_B\left|\beta^x{}_{,x}\right|\tilde{\Gamma}^x + \cdots \ , \quad (11)$$

and similarly for $\tilde{\Gamma}^y$ and $\tilde{\Gamma}^z$. Note that the "exponential" terms in the above equation (i.e. the terms proportional to $\tilde{\Gamma}^x$) are now guaranteed to be exponential *decay* terms. We find good results with $\lambda_A = 2/3$ and $\lambda_B = 3/4$.

Alcubierre *et al.* [62] find improved behavior when they enforce the constraint $\mathcal{T} = 0$. Yo *et al.* [12] found it useful to enforce $\mathcal{T} = \mathcal{D} = 0$. We instead apply the reasoning above to modify the evolution equations for $\tilde{\gamma}_{ij}$ and $\tilde{A}_{ij}$. Thus, in the equation for $\tilde{\gamma}_{xx}$, we find the terms

$$\partial_t \tilde{\gamma}_{xx} = \left(-\frac{2}{3}\beta^j{}_{,j} + 2\beta^x{}_{,x} \right) \tilde{\gamma}_{xx} + \cdots \tag{12}$$

which we replace by

$$\begin{aligned} \partial_t \tilde{\gamma}_{xx} \;=\; & \frac{2}{3}\left[-\beta^j{}_{,j} + \lambda_C \left|\beta^j{}_{,j}\right| \right] G_{xx} - \frac{2}{3}\lambda_C \left|\beta^j{}_{,j}\right| \tilde{\gamma}_{xx} \\ & + 2\left[\beta^x{}_{,x} + \lambda_D \left|\beta^x{}_{,x}\right| \right] G_{xx} - 2\lambda_D \left|\beta^x{}_{,x}\right| \tilde{\gamma}_{xx} \\ & + \cdots \ , \end{aligned} \tag{13}$$

where G_{xx} is the value of $\tilde{\gamma}_{xx}$ as computed from the five other independent components of $\tilde{\gamma}_{ij}$, assuming $\mathcal{D} = 0$. We perform the same substitution for $\tilde{\gamma}_{yy}$ and $\tilde{\gamma}_{zz}$. We use $\lambda_C = 2/3$ and $\lambda_D = 1/10$. In a similar fashion, we modify the evolution of $\tilde{A}_{xx}$, $\tilde{A}_{yy}$, and $\tilde{A}_{zz}$ from

$$\partial_t \tilde{A}_{xx} = \cdots + \left(-\frac{2}{3}\beta^j{}_{,j} + 2\beta^x{}_{,x} + \alpha K \right) \tilde{A}_{xx} \tag{14}$$

to

$$\begin{aligned} \partial_t \tilde{A}_{xx} \;=\; & \frac{2}{3}\left[-\beta^j{}_{,j} + \lambda_C \left|\beta^j{}_{,j}\right| \right] H_{xx} - \frac{2}{3}\lambda_C \left|\beta^j{}_{,j}\right| \tilde{A}_{xx} \\ & + 2\left[\beta^x{}_{,x} + \lambda_D \left|\beta^x{}_{,x}\right| \right] H_{xx} - 2\lambda_D \left|\beta^x{}_{,x}\right| \tilde{A}_{xx} \\ & + \left[\alpha K + \lambda_E \left|\alpha K\right| \right] H_{xx} - 2\lambda_E \left|\alpha K\right| \tilde{A}_{xx} \\ & + \cdots \ , \end{aligned} \tag{15}$$

and similarly for the other two components. Here $\lambda_E = 0.1$, λ_C and λ_D are the same as above, and H_{xx} is the value of $\tilde{A}_{xx}$ computed from the five other independent components of $\tilde{A}_{ij}$ assuming $\mathcal{T} = 0$.

We take spatial derivatives in a centered way—we do not use causal differencing. The only exception, as suggested by [11], is in the advection terms along the shift $\beta^i \partial_i$, for which we use the second-order upwind differencing described in [63].

Our hydrodynamics scheme uses van-Leer type advection and artificial viscosity shock handling [24]. It is known that such schemes can be inaccurate for ultra-relativistic flows [64]. We monitor the Lorentz factors of our fluids, and find that they never exceed ≈2, which is around the upper limit for accurate evolutions with a van Leer code. In addition, most of our runs do not involve strong shocks. We thus believe that our hydrodynamics scheme is adequate for the present purposes, although we eventually may have to improve it. Our hydrodynamics scheme employs the "no atmosphere" approach [24], so that the density at any point on our grid is allowed to fall to zero. It is important that we are able to dispense with an artificial atmosphere. If we could not, then in situations where all the matter in the problem falls into the black hole, the hole would continue to accrete atmosphere indefinitely, and its mass would continue to grow unphysically.

The boundary conditions we apply at the edge of the excision zone are described in detail in [12]. They consist of taking the time derivatives of quantities at the excision boundary from the time derivatives of these quantities at adjacent points. We use spherical excision regions inside the apparent horizon throughout (see [65] regarding the superiority of spherical to cubic excision regions). We have tried several boundary conditions for the matter variables, and have found that our results are insensitive to the choice, as they should be. In the runs described below, we simply set the matter variables equal to zero when they hit the excision zone, thus making the excision boundary a perfect one-way membrane.

The lapse and shift must be chosen in such a way that the total system of evolution equations is stable. It is also desirable that the gauge conditions are chosen so that, as the system settles into equilibrium, it appears stationary in the adopted coordinates. We have experimented with several choices for the lapse α and shift β^i, and we have found that driver conditions using the second time derivatives of α and β^i provide the most stable evolutions. Following the suggestion of Alcubbierre *et al* [17], we have had great success with the hyperbolic shift driver condition:

$$\partial_t^2 \beta^i = b_1(\alpha \partial_t \tilde{\Gamma}^i - b_2 \partial_t \beta^i) \ , \tag{16}$$

with $b_1 = 0.75$ and $b_2 = 0.27M^{-1}$ (c.f. [11]). One can create a hyperbolic lapse condition by introducing two coupled first-order equations and a new function $\mathcal{A}$

$$\begin{aligned} \partial_t \alpha \;&=\; \alpha \mathcal{A} \\ \partial_t \mathcal{A} \;&=\; -a_1(\alpha \partial_t K + a_2 \partial_t \alpha) \ , \end{aligned} \tag{17}$$

with $a_1 = 0.75$ and $a_2 = 0.27M^{-1}$. The α in front of $\mathcal{A}$ in the first equation is a "safety" feature, to prevent the lapse from dropping to zero. With this safety feature, we find that the lapse levels off at finite positive values everywhere on and outside the excision zone for all our runs, thereby maintaining a "horizon penetrating" ($\alpha > 0$) time coordinate. However, at late times ($t \sim 200M$), we find that the asymptotic values of some of our variables (e.g. $\tilde{\gamma}_{xx}$) begin to drift, increasing linearly with time. This drift is also present when harmonic slicing, another slicing with a hyperbolic character [66], is adopted. Apparently, Eq.(17) does not sufficiently restrict the coordinate system's evolution. We remove the drift by adding a third term to Eq.(17) proportional to $K - K_{\rm drive}$, where $K_{\rm drive}$ is some reasonable positive function. In this way, the value of K itself, and not just its time derivative, is "driven". We shall refer to this slicing as our "hyperbolic lapse". The complete slicing condition

is

$$\begin{aligned}\partial_t \alpha &= \alpha \mathcal{A} \\ \partial_t \mathcal{A} &= -a_1(\alpha \partial_t K \\ &\quad + a_2[\partial_t \alpha + e^{-4\phi}\alpha(K - K_{\rm drive})]) \ . \end{aligned} \tag{18}$$

Here the $e^{-4\phi}\alpha$ factor is chosen so that the new term is small in the strong-field region, where (17) works well, but becomes comparable to the other terms in the outer portions of the grid, where it successfully removes the drift.

We have tried several forms for $K_{\rm drive}$. The simplest, and usually adequate choice, is zero. This drives K to zero (maximal slicing) and usually causes a very slow downward drift in the lapse near the horizon. For many astrophysical applications, where we only need to evolve for several hundred M, this is usually unimportant. However, the effect can be removed by a better choice of $K_{\rm drive}$. One possibility is $K_{\rm init}$, the value of K at the time excision is introduced. Another choice is K_{KS}, a function whose form is inspired by the Kerr-Schild representation of a Kerr black hole [c.f. Eq. (36) of [12]].

$$\begin{aligned} K_{KS}(\alpha,\beta^i) &= 2\alpha^3(1+H)l^i H_{,i} + 2\alpha H l^i{}_{,i} \\ H &= \frac{1}{2}(\alpha^{-2}-1) \\ l^i &= \beta^i/(2\alpha^2 H) \end{aligned} \tag{19}$$

Note that when we choose this functional form for K_{KS}, the lapse and shift typically are not the same as the Kerr-Schild α and β^i.

For $K = K_{\rm drive}$, we apply our usual excision boundary conditions on α. Otherwise, there are no spatial derivatives in Eq. (18), and no explicit inner boundary condition is needed. In some cases, however, we have found more accurate results when we hold the values of the lapse on the excision zone fixed in time (the "frozen" inner boundary condition).

III. DIAGNOSTICS

Our most important diagnostics are the conserved mass M and angular momentum J. These are both defined by surface integrals at infinity [67]:

$$M = \frac{1}{16\pi}\int_{r=\infty} \sqrt{\gamma}\gamma^{im}\gamma^{jn}(\gamma_{mn,j} - \gamma_{jn,m}) d^2S_i \tag{20}$$

$$J_i = \frac{1}{8\pi}\varepsilon_{ij}{}^k \int_{r=\infty} x^j K^m_k d^2 S_m. \tag{21}$$

We measure M and J by applying Gauss' Law to obtain a surface integral over an inner surface, $\partial\Omega$, (which encloses the singularity) plus a volume integral over the space outside this surface, Ω. Details of this calculation are presented in [12]. The final integrals are

$$\begin{aligned} M &= \frac{1}{16\pi}\int_\Omega d^3x \Big[e^{5\phi}\Big(16\pi\rho + \tilde{A}_{ij}\tilde{A}^{ij} - \frac{2}{3}K^2\Big) \\ &\qquad - \tilde{\Gamma}^{ijk}\tilde{\Gamma}_{jik} + (1-e^\phi)\tilde{R}\Big] \\ &\quad + \frac{1}{16\pi}\oint_{\partial\Omega}(\tilde{\Gamma}^i - 8\tilde{D}^i e^\phi) d\tilde{S}_i \end{aligned} \tag{22}$$

$$\begin{aligned} J_i &= \frac{1}{8\pi}\epsilon_{ij}{}^k \int_\Omega \Big[e^{6\phi}\Big(\tilde{A}^j{}_k + \frac{2}{3}x^j\tilde{D}_k K \\ &\qquad - \frac{1}{2}x^j\tilde{A}_{ln}\partial_k\tilde{\gamma}^{ln} + 8\pi x^j s_k\Big)\Big] d^3x \\ &\quad + \frac{1}{8\pi}\epsilon_{ij}{}^k \oint_{\partial\Omega} e^{6\phi} x^j \tilde{A}^l{}_k d\tilde{S}_l. \ . \end{aligned} \tag{23}$$

We choose the inner surface $\partial\Omega$ to be a sphere with a coordinate radius about twice that of the excision boundary. This puts $\partial\Omega$ slightly outside the apparent horizon in the simulations reported below.

In our pre-excision code, Ω is chosen to cover the entire numerical grid, and there is no surface integral contribution. The rest mass M_0 cannot be used as a diagnostic because it is conserved identically in our pre-excision code. Our pre-excision code also conserves J identically in axisymmetry [44]. With excision, M_0 is not expected to be conserved in Ω, since matter falls into the excision region. When evolving with excision, J is not identically conserved, even in axisymmetry, and thus serves as a code check together with M.

Once a black hole is present, we detect it by using an apparent horizon finder (see [68] for details). As the system approaches stationarity, the apparent horizon will approach the event horizon. We estimate the size the horizon in our coordinate system by the radius $r_{\rm AH}$ constructed from the $l = 0$, $m = 0$ moment of the horizon surface. From the surface area of the apparent horizon, we compute the irreducible mass $M_{\rm irr}$ defined by

$$M_{\rm irr} = \sqrt{\mathcal{A}/16\pi^2} \tag{24}$$

We also compute the proper circumference of the horizon in the equatorial (xy) plane, which we call $C_{\rm eq}$, and we compute the proper circumference in the meridional (xz) plane, which we call $C_{\rm pol}$. For static nonrotating black holes, $C_{\rm eq} = C_{\rm pol} = 4\pi M$. For stationary rotating black holes, one can compute $C_{\rm eq}$ and $C_{\rm pol}$ from the Kerr metric in Boyer-Lindquist coordinates to be

$$C_{\rm eq} = 4\pi M \tag{25}$$

$$C_{\rm pol} = 4M\int_0^{\pi/2} d\theta \sqrt{2 + 2\sqrt{1-q^2} + q^2\sin^2\theta} \ , \tag{26}$$

where $q \equiv J/M^2$ is the spin parameter of the black hole. The ratio $C_{\rm pol}/C_{\rm eq}$ varies from 1 for $q = 0$ to 0.6 for $q = 1$. For the black holes in our simulations, we infer the horizon mass $M_{\rm AH}$ from $C_{\rm eq}$ and Eq. (25). We infer

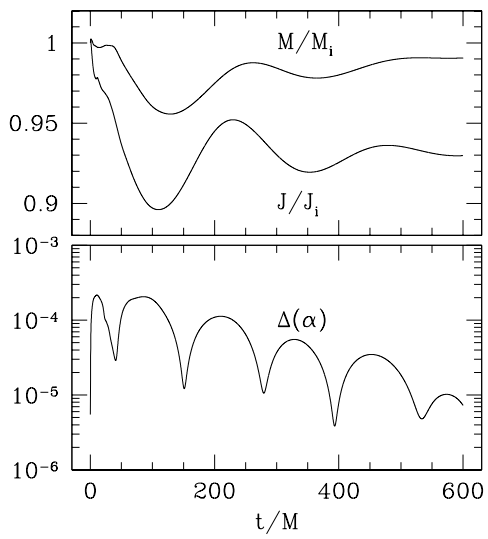

FIG. 1: The evolution of the mass M, angular momentum J, and lapse variation $\Delta\alpha$ for the evolution of an $a/M = 0.4$ black hole in Kerr-Schild coordinates. We use a 30^2 grid to cover the meridional plane..

the horizon angular momentum $J_{\rm AH}$ from $C_{\rm pol}/C_{\rm eq}$ and Eq. (26), together with $M_{\rm AH}$.

Finally, we find the ergosurface of the black hole. The ergosphere is defined in the stationary limit, in which case $\frac{\partial}{\partial t}$ is a Killing vector, and the ergosurface is defined as the surface where $g_{00} = \frac{\partial}{\partial t}\cdot\frac{\partial}{\partial t} = 0$, with $g_{00} > 0$ inside and $g_{00} < 0$ outside.

As in [11, 12], we gauge the degree to which a field f reaches stationarity by monitoring $\Delta f(t)$, defined to be the L2 norm of $f(t) - f(t - \Delta T)$, where ΔT is the timestep. We compute the L2 norm of a gridfuntion g by summing over every gridpoint i:

$$L2(g) = \sqrt{\sum_i g_i^2} \qquad (27)$$

IV. TESTS

A. Field Code Test: Vacuum Black Holes

In a previous paper [12], we used our code to evolve isolated, stationary black hole spacetimes in Kerr-Schild coordinates. These coordinates have the advantages of being horizon-penetrating ($\alpha \neq 0$ at the horizon) and providing a manifestly stationary metric. We were able to evolve both stationary and rotating black holes for arbitrarily long times. We succeeded in doing this both when evolving only one octant of the space and when evolving the full space without any symmetry assumptions. These evolutions were done in three dimensions using a different set of gauge conditions from those utilized in this paper. In Figure 1, we show the evolution of a $a/M = J/M^2 = 0.4$ Kerr black hole in Kerr-Schild coordinates using our 2D axisymmetry code and our hyperbolic gauge conditions. For this case, we use a frozen inner boundary condition on α, and turn off the third term in (18). (Using $K_{\rm drive} = K_{\rm init}$ gives similar results.) We use a grid spacing of $\Delta X = 0.4M$, with outer boundaries at $12M$ and an excision zone at a coordinate radius of $1.5M$, as was used by [12]. The event horizon for $a/M = 0.4$ is located at $r_{\rm eq} = 1.917M$ in these coordinates.

As a second test, adapted from [11], we evolve a Schwarzschild black hole in initially isotropic coordinates. Choosing $\alpha = 1$ and $\beta^i = 0$ at $t = 0$, the initial metric is

$$ds^2 = -dt^2 + \left(1 + \frac{2M}{r}\right)(dx^2 + dy^2 + dz^2)\ , \qquad (28)$$

where $r = \sqrt{x^2 + y^2 + z^2}$. The event horizon is located at $r = 0.5M$ in these coordinates. Physically, this black hole is stationary, but it does not appear stationary in the coordinates generated by Eqns. (16) and (18) starting with the initial lapse and shift cited above. By evolving this spacetime, we check that our excision code can work with coordinates other than stationary Kerr-Schild. We also check the ability of our gauge conditions to "find" coordinate systems which make the metric manifestly stationary. We allow the lapse to drop, so we do not freeze the lapse at the excision zone, but employ equation (18) everywhere. We use $K_{\rm drive} = K_{\rm init} = 0$, since K_{KS} is singular for our value of α at $t = 0$ [see equation (19)].

In Figure 2, we plot the results for a run in axisymmetry with outer boundaries at $12M$, an excision radius of $0.36M$, and a grid of 128^2 to cover the meridional (xz) plane. Also shown are scaled results for a 64^2 run to demonstrate convergence. We also performed a run on a 256^2 grid with the same resolution as the 128^2 run but with the outer boundaries at $24M$. From the figure, we see that the error can be controlled by the grid resolution and the location of the outer boundaries. We see that the surface area of the apparent horizon (i.e. $M_{\rm irr}$) remains nearly constant while the coordinates adjust to create a stationary system. This indicates that the apparent horizon is following the event horizon well. The coordinate adjustment is reflected in the initial increase in the coordinate radius of the horizon and in the drop of the lapse. Note that the lapse settles quickly, and that it remains positive everywhere outside and at the excision zone. To check that the black hole remains a Schwarzschild black hole, we monitor $C_{\rm eq}$ and $C_{\rm pol}$ and find that they both remain equal to $4\pi M$ to within one percent.

B. Hydro Code Test: Relativistic Bondi Flow

Next, we test our hydrodynamics code by solving an accretion problem that has an exact solution. In a previous paper [24], we confirmed our code's ability to accurately simulate shocks, spherical dust collapse, nonro-

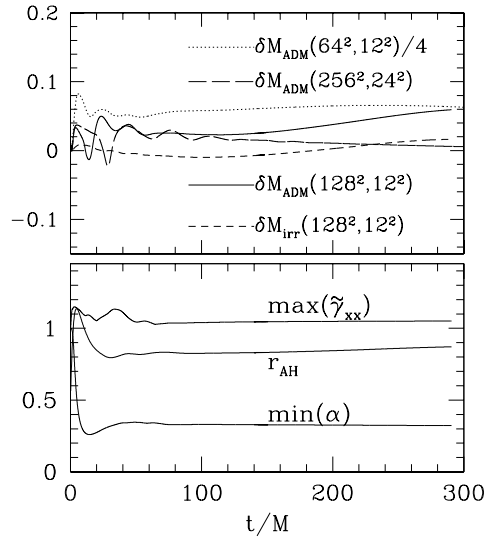

FIG. 2: The evolution of a nonrotating black hole in our hyperbolic gauges, starting in isotropic coordinates with $\alpha = 1$, $\beta^i = 0$. On top, we show the deviations of the ADM mass $M_{\rm ADM}$ and the irreducible mass $M_{\rm irr}$ from their initial value: $\delta M = (M - M_i)/M_i$. δM is shown for runs with outer boundaries at $12M_i$ using a 128^2 grid and using a 64^2 grid, to demonstrate convergence. We also show a run with outer boundaries at $24M_i$ using a 256^2 grid to determine the effect of the outer boundary. Below, we show the time evolution on the 128^2 grid of the apparent horizon coordinate radius $r_{\rm AH}$ and the maximum values of α and $\tilde{\gamma}_{xx}$ on the grid.

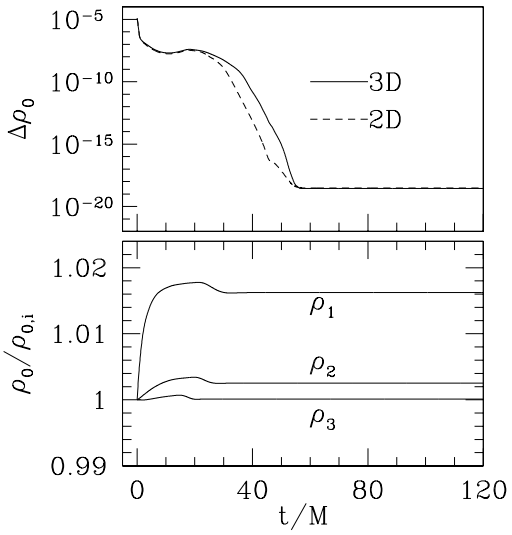

FIG. 3: The settling of the rest-mass density to steady-state, starting from the analytic value. The change per timestep quickly drops to the machine level. On top, we plot $\Delta\rho_0$ for both the 64^2 2D run and the 64^3 3D run. Below, we show the time evolution of ρ_0 at three points on the diagonal line $x = y = z$ in the 3D run, each normalized to its initial value. ρ_1 corresponds to ρ_0 measured at $r = \sqrt{3}x = 2M$, ρ_2 to ρ_0 at $r = 6M$, and ρ_3 to ρ_0 at $r = 10M$.

tating and rotating polytropes, and binary polytropes. Now we test its ability to maintain stationary, adiabatic, spherically symmetric accretion onto a Schwarzschild black hole, in accord with the relativistic Bondi accretion solution for $\Gamma = 1.5$ [69]. Following the suggestion of [70], we write the metric in Kerr-Schild (ingoing Eddington-Finklestein) coordinates; in this way, all the variables are well behaved at the horizon. We begin by holding the field variables fixed in order to prevent the black hole from growing due to accretion.

We evolve this system twice, once using a 64^2 grid in 2+1 and once using a 64^3 grid in 3+1. We place outer boundaries at $12M$ and an excision zone at a coordinate (areal) radius of $1.5M$. At $t = 0$, we set the density and velocity profiles according to the exact solution for $\Gamma = 1.5$ and an accretion rate $dM/dt|_{\rm acc} = 0.0031$, with a sonic radius at $10^5 M$. This accretion rate is maintained through the evolution by fixing the hydrodynamic variables on the outer boundaries at their exact steady-state values. In Figure 3, we plot $\Delta(\rho_0)$, as defined in Section III, and also the values of ρ_0 at selected points in the accretion flow. For $\Delta(\rho_0)$, we reach machine precision after less than $100M$, making further integration unnecessary [12]. (The velocity fields have also frozen near their initial values by this time.)

When we allow the fields to evolve, we see the irreducible mass of the hole grow at a rate $dM_{\rm irr}/dt \approx 0.9 dM/dt|_{\rm acc}$. This error is consistent with the errors in our irreducible mass found at this numerical resolution, even in the absence of accreting matter.

C. Oppenheimer-Snyder Collapse

Next, we simulate the Oppenheimer-Snyder collapse of a homogeneous spherical ball of dust to a black hole. The behavior of this system is known in several coordinate systems [71, 72, 73]. We use a 160^2 grid with outer boundaries at $14M$. At $t = 0$, the dust is at rest and has an areal radius of $3M$. We start in an isotropic coordinate system, in which $\tilde{\gamma}_{ij} = \delta_{ij}$. Our initial α and β^i are set by enforcing maximal slicing and the minimal distortion gauge condition, respectively (see [72]). Since the ball has no pressure support, it immediately begins to collapse. During the first phase of this collapse, there are no trapped regions and no singularities, so we evolve the entire grid without excision. Our code checks during this part of the evolution are well satisfied; see [24, 44]. For gauge conditions during this no-excision phase, we use our hyperbolic lapse and shift drivers. We evolve in this way from $t = 0$ to $t = 11M$, at which point our no-excision code crashes due to its inability to resolve the central region ("grid stretching"). An apparent horizon appears at $t = 9M$ at a coordinate radius of $r_{\rm AH} = 0.96M$ with an irreducible mass of $M_{\rm irr} = 1.02M$. We next repeat the evolution from $t = 10M$ with our

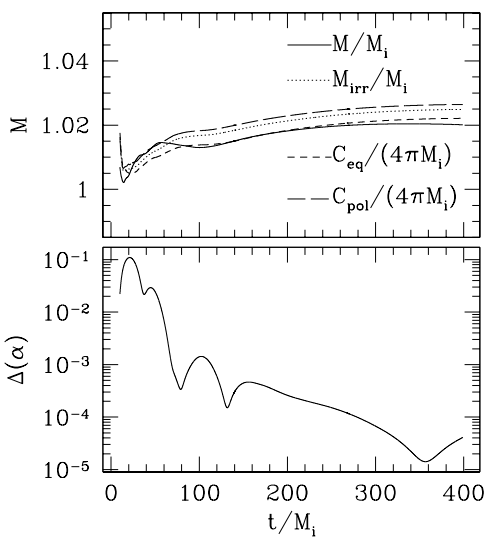

FIG. 4: ADM mass, horizon diagnostics, and $\Delta\alpha$ for the collapse of a homogeneous sphere of dust to a Schwarzschild black hole. Collapse begins at $t = 0$ and black hole excision occurs at $t = 10M$.

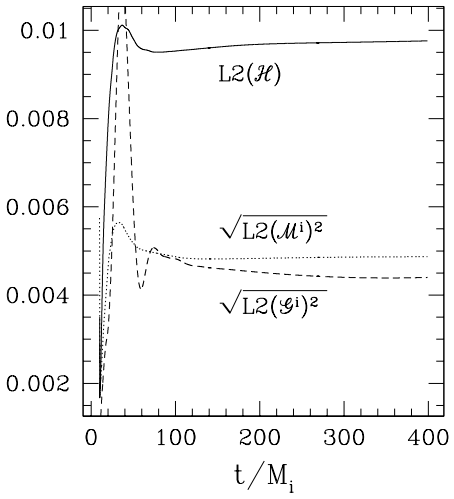

FIG. 5: Violation of the Hamiltonian $\mathcal{H}$, momentum $\mathcal{M}^i$, and Gamma $\mathcal{G}^i$ constraints as a function of time for the collapse depicted in Fig. 4. We plot the un-normalized L2 norms, where we use the shorthand $L2(\mathcal{M}^i)^2 = L2(\mathcal{M}^x)^2 + L2(\mathcal{M}^y)^2 + L2(\mathcal{M}^z)^2$ and $L2(\mathcal{G}^i)^2 = L2(\mathcal{G}^x)^2 + L2(\mathcal{G}^y)^2 + L2(\mathcal{G}^z)^2$.

excision algorithm and an excision boundary at radius $r_{\rm ex} = 0.7M$. At this point, only 1.2% of the rest mass is outside the horizon, but the spacetime in our coordinates is still changing. We continue to evolve with our hyperbolic gauges, and we allow α to drop at the excision boundary. In this example, using $K_{\rm drive} = K_{\rm KS}$ is far superior to any other choice, since only then does the lapse

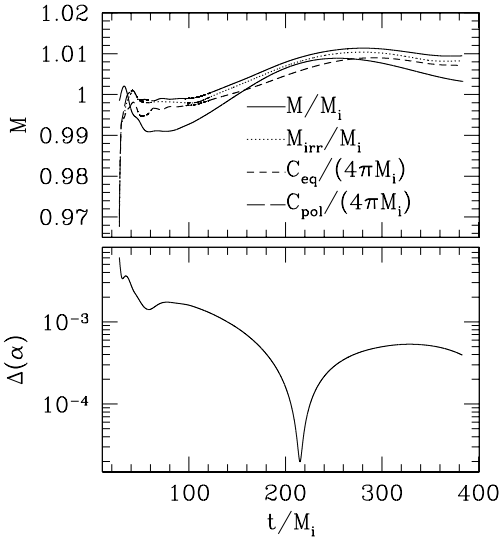

FIG. 6: ADM mass, horizon diagnostics, and $\Delta\alpha$ for the collapse of a nonrotating, unstable $n = 1$ polytrope from apparent horizon formation at $t/M = 27$ through final stationarity. The code is axisymmetric and uses a 128^2 grid.

settle quickly. As we continue the evolution, the remaining exterior rest mass falls into the excision zone over the course of the next $100M$, and we are left with a vacuum spacetime. We evolve for $400M$, by which time the system has long since settled to a Schwarzschild black hole. Oppenheimer-Snyder collapse does have an analytic solution in Friedmann coordinates, but not in the coordinates we are using, which are defined by our gauge conditions (16) and (18) together with the boundary conditions on α and β^i at $r_{\rm ex}$. Therefore we check the accuracy of our evolution using global invariants. In Figure 4, we show our mass diagnostics for the post-excision run, which confirm that the end product is a Schwarzschild black hole, and we plot $\Delta\alpha$ as proof of stationarity. In Figure 5, we plot the magnitude of the constraint violations as functions of time. These show that the error is not growing during the long stationary evolution.

D. Collapse of a TOV Star

The previous example possessed spherical symmetry and no pressure. In our next test, we study the collapse of an unstable nonrotating, spherical polytrope, whose initial state is given by the solution to the TOV equations [74].

For initial data, we take a perfect fluid with equation of state $P = \kappa\rho_0^{1+1/n}$, with $n = 1$, and we choose our units such that $\kappa = 1$ [75]. In these units, the $n = 1$ TOV sequence has a turning point at the critical central rest density $\rho_c^{\rm crit} = 0.32$ where the ADM mass of the star is $M_{\rm max} = 0.164$. We choose to evolve a star with initial central rest density $\rho_c = 0.5$ and ADM mass $M =$

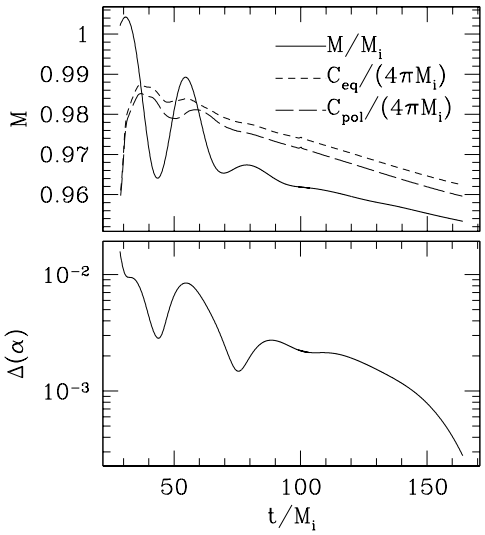

FIG. 7: Same as for Figure 6, but now the collapse is simulated on a 3D 64^3 grid.

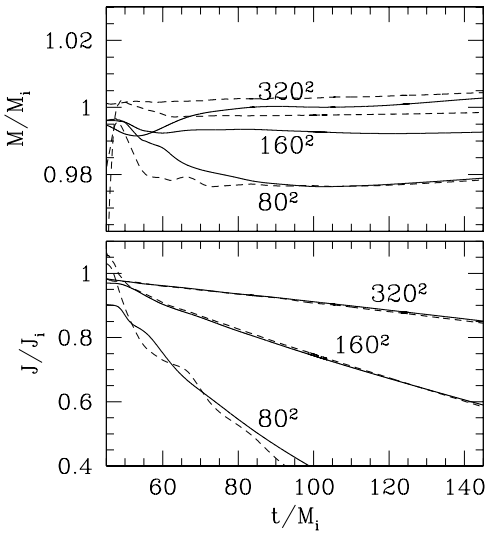

FIG. 8: Mass M and angular momentum J during the post-excision phase of the collapse of star A. We show results for axisymmetric runs carried out with a 80^2, a 160^2, and a 320^2 grid. Both M and J are measured in two ways. The solid lines are quantities as measured by the integrals (22) and (23). The dashed lines are obtained by measuring the geometry of the apparent horizon and comparing with the Kerr metric ($M_{\rm AH}$ as inferred by $C_{\rm eq}$ and $J_{\rm AH}$ by $C_{\rm pol}/C_{\rm eq}$). For the 160^2 and 320^2 runs, the two J measurements lie on top of one another.

0.158. As this star is on the unstable branch of the $n = 1$ sequence, it is unstable to radial oscillations and will collapse to a black hole. We evolve the first part of the collapse without excision using a 128^2 grid, with outer boundaries at $12.7M$ and with our hyperbolic drivers. We evolve from $t = 0$ to $t = 28.5M$, locating an apparent horizon at $t = 27M$ with radius $r = 0.6M$ and irreducible mass $M_{\rm irr} = 0.95M$. We begin an excision run from $t = 27.8M$, at which point 4% of the rest mass is still outside the apparent horizon and 8% is outside of the excision zone. All of this matter falls into the excision zone by $t = 31.6M$. It should be emphasized that the spacetime in these coordinates is more dynamical than the above numbers might suggest: e.g. during the first $10M$ of post-excision evolution, the maximum value of $\tilde{A}^{ij}\tilde{A}_{ij}M^2$ increases from 0.25 to 0.44. The system settles quickly thereafter, as we see by evolving an additional $350M$ to $390M$. In Figure 6, we show our diagnostics for this run.

All the runs described above were carried out on two-dimensional axisymmetric grids. In Figure 7, we show diagnostics for the same collapse in a three dimensional simulation, with a 64^3 grid and boundaries at $[0, 12.7M]^3$ (employing octant symmetry to evolve only the upper octant). The behavior of each quantity is similar to that in the 2D run.

E. Collapse of a Rotating Star

Gravitational collapse of astrophysically realistic stars will involve rotation. Even if the progenitor star rotates slowly, it will spin up as it collapses if it conserves angular momentum. It is therefore important to test our code by simulating the collapse of a rapidly rotating star.

The star we adopt as initial data, labeled A, is described in Table I. The initial data was obtained using the relativistic equilibrium code of [76]. Star A is a "hypermassive star" with a mass $M = 0.19$, which is 20% higher than $M_{\rm max}$, the maximum allowed mass of a non-rotating TOV star. Star A is able to maintain this mass because of the added support against gravity provided by (differential) rotation. The star has $J/M^2 = 0.57$, so that the eventual Kerr hole will have appreciable spin, assuming all of the mass and angular momentum is captured by the hole. Even prior to collapse, the effects of angular momentum on the star are significant, as we can see by noting that the radius of the star on the rotation z-axis (the polar radius) is only 70% of the radius of the star in the equatorial plane (the equatorial radius). Star A has a differential rotation profile (see next section), so there are no turning-point theorems which can be applied to determine the stability of this star, but we find numerically that it is unstable to collapse. Perturbations due to numerical (roundoff) error are sufficient to trigger the collapse, but the onset timescale for collapse is not independent of resolution. In order to do convergence studies, we deplete a small percentage (4%) of the initial pressure, so that the initial perturbation is resolution-independent. This perturbation is so small that re-solving the constraint equations at $t = 0$ makes little difference.

We carry out the entire evolution, before and after exci-

sion, in the hyperbolic gauges. (The choice of $K_{\rm drive}$ has a negligible effect on the evolution in this application.) We perform the same evolution on a 80^2 grid, a 160^2 grid, and a 320^2 grid. On the 320^2 grid, a horizon appears in the pre-excision run at $t = 44M$, with instantaneous radius $r_{\rm AH} = 0.5M$ and mass $M_{\rm irr} = 0.77M$, which are growing rapidly. We excise at time $t = 45.5M$ and radius $r_{\rm ex} = 0.43M$, so that 22% of the total rest mass is still outside the excision region, and 12% is still outside the apparent horizon (which now has radius $r_{\rm AH} = 0.73M$). This matter quickly falls into the hole, and, after evolving for $6M$ with excision, the exterior spacetime becomes a vacuum. In Figure 8, we check the ability of our code to conserve mass and angular momentum during this phase of the evolution. The mass is well conserved on all three grids, but the angular momentum slowly decreases with time. Increasing resolution reduces this loss of J. The violations of the constraint equations also converge to zero as resolution is increased. We can evolve stably for $t \gg 100M$, but the loss of angular momentum is too great past this point for the evolution to be reliable unless the grid exceeds 320^2.

Figure 8 suggests that the angular momentum loss can be controlled by increasing resolution. Moreover, we have already shown that our code can conserve J for an arbitrarily long time while evolving a Kerr black hole in Kerr-Schild coordinates (see Fig. 1 and [12]). Given this fact, we could eliminate the J loss by transforming to Kerr-Schild coordinates when we introduce excision. Alternatively, we might carry out the entire evolution in Kerr-Schild-like coordinates. (This would require developing gauge conditions which would force the coordinate-system to maintain its Kerr-Schild-like character as the system evolves.) We are currently investigating these possibilities. In the meantime, we can already evolve such matter-black hole systems long enough to tackle several interesting problems.

V. APPLICATION: THE COLLAPSE OF RAPIDLY ROTATING STARS

Tracking the collapse of rapidly rotating stars is one of the most important applications of numerical general relativity. Such simulations determine the fate of collapse and provide a test of the cosmic censorship conjecture [77]. If the star collapses to a stationary black hole, the "no-hair" theorems require that it settle down to a Kerr black hole. In the Kerr spacetime, the singularity is covered by an event horizon only if $q \equiv J/M^2 \leq 1$; otherwise the singularity is naked. Rotating stars, on the other hand, are not so restricted, and sufficiently rapidly rotating stars will have $q > 1$. When these stars collapse, it thus seems conceivable that they could form naked singularities. Alternatively, if the cosmic censorship hypothesis [77] is true, then the collapse of the whole system must somehow be averted. This can happen if the star loses angular momentum as it collapses, either by gravitational wave emission or by shedding matter with high specific angular momentum, so that the final black hole has $q < 1$. A naked singularity can also be averted if the collapse of a $q > 1$ star is always halted by centrifugal forces, so there will be no black hole and no singularity at all. Nakamura [78] has pointed out that a centrifugal barrier could protect cosmic censorship in this way. Assuming no mass or angular momentum are shed during the collapse, the radius R_b at which the centrifugal force balances the gravitational force will be

$$\frac{M}{R_b^2} \sim \frac{J^2}{M^2 R_b^3} \ , \tag{29}$$

so that

$$R_b \sim M q^2 \ . \tag{30}$$

Nakamura argues that, if $q < 1$ (i.e., the star is *subKerr*), the star will already be inside a black hole before rotation can halt the collapse. For $q > 1$ (i.e., the star is *supraKerr*), the collapse will be halted at a radius larger than M, and no black hole forms.

Shapiro and Teukolsky [54] have studied the collapse in full general relativity of axisymmetric tori consisting of collisionless matter, and have found that black holes form only from subKerr initial configurations. The first numerical simulations of the collapse of rotating relativistic fluid stars were carried out in axisymmetry by Nakamura [79] and Nakamura and Sato [80]. They found that a black hole forms only when a subKerr star collapses. (For stars with q within 5% of the critical value, Nakamura [79] could not determine the final fate and could not exclude the possibility of a naked singularity.) Stark and Piran [81] also performed simulations which showed $q \sim 1$ to be the critical point of demarcation between collapse and bounce. Shibata [27] performed a detailed study of the collapse and bounce of subKerr stars in axisymmetry. These hydrodynamic studies did not (and sometimes could not) study in detail the fate of the matter in the outer layers of the star when a black hole forms. More recently, Shibata [28] has studied the collapse to black

TABLE I: Equilibrium Star Configurations ($n = 1$, $M_0 = 0.2$).

Star	M^a	$R_{\rm eq}{}^b$	$R_c{}^c$	q^d	$T/\lvert W\rvert^e$	$\Omega_c/\Omega^f_{\rm eq}$	$\mathcal{R}^g$	Fate^h
A	0.19	0.6	0.8	0.57	0.10	0.29	0.70	BHND
B	0.19	1.2	1.4	0.91	0.18	0.38	0.50	BHND
C	0.19	1.6	1.8	1.18	0.23	0.40	0.39	NBH

[a] ADM mass
[b] coordinate equatorial radius
[c] areal radius at the equator
[d] $q = J/M^2$
[e] ratio of kinetic to gravitational potential energy
[f] ratio of central to equatorial angular velocity
[g] ratio of polar to equatorial coordinate radius
[h] BHND = black hole, no disk; NBH = no black hole

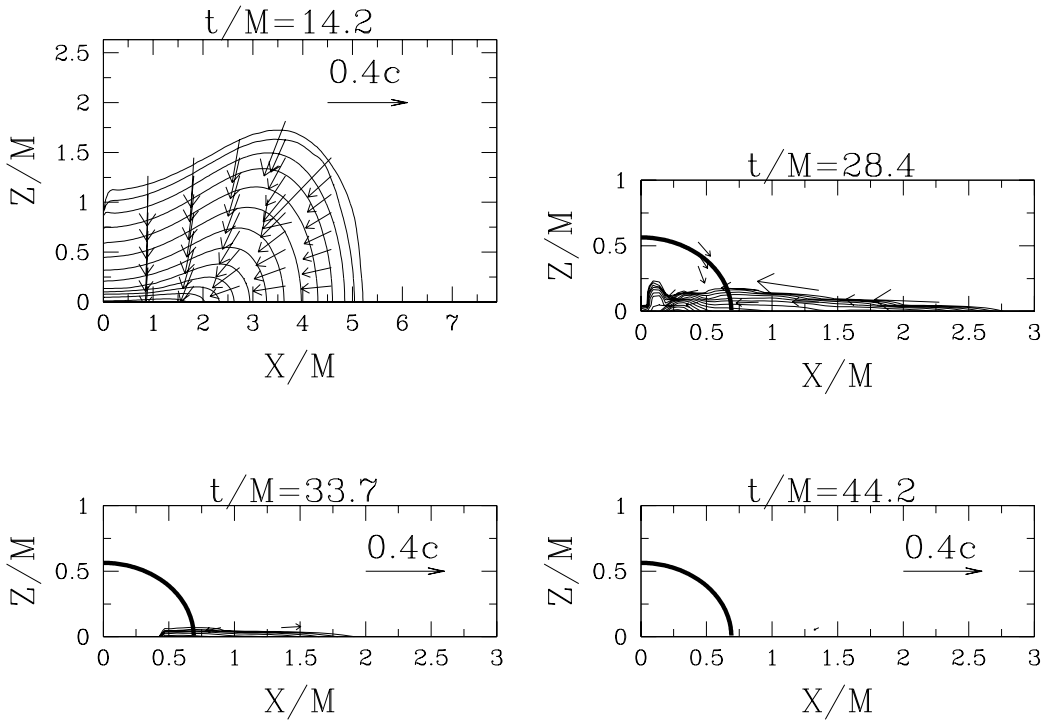

FIG. 9: Snapshots of the rest-density contours and the velocity field (v^x, v^z) in the meridional plane during the collapse of star B to a black hole. The contour lines are drawn for $\rho_0 = 10^{-(0.2\ j+0.1)}\rho_0^{Max}$ for $j = 0, 1, .., 12$. Prior to excision, ρ_0^{Max} is set equal to the instantaneous maximum value of ρ_0. Afterwards, it is held at the maximum of ρ_0 at the time of excision. Vectors indicate the local velocity field, v^i. The thick curve in the last three frames marks the apparent horizon. On the last frame, the exterior spacetime is nearly a vacuum.

holes of uniformly rotating polytropes spinning at the mass-shedding limit. He finds that, for polytropic indicies $2/3 < n < 2$, the star collapses to a Kerr black hole with no appreciable disk. By using high resolution, he is able to follow the system for $\Delta t \sim 20M$ after an apparent horizon is first located. This time approaches the limit of reliable evolution without excision, but in this case it is long enough to see all the matter fall into the hole. By contrast, Shibata and Shapiro [29] considered the collapse of an $n = 3$ polytrope spinning uniformly at the mass-shedding limit. Such a configuration is nearly Newtonian ($R_{\rm eq} = 620M$) at the onset of collapse, and it forms an appreciable disk ($M_{\rm D}/M \approx 0.1$) around the final black hole. While the final disk mass can be estimated from the angular momentum distribution of the outermost regions (see also [82]), and also by extrapolating the growth of the black hole horizon to late times, it is not possible to follow the final relaxation to a stationary state without excision or to probe for nonaxisymmetric instabilities that may arise in the ambient disk [47]

Our excision code should be well suited to finding the final state of any rapidly rotating stellar collapse—not only for determining whether or not a black hole forms, but also for determining how much rest mass escapes collapse if one does form. To explore this capability, we take differentially rotating polytropes as our initial data, so that we can study both subKerr and supraKerr cases. Differential rotation is naturally produced in supernova core collapse [83], accretion induced collapse of white dwarfs to neutron stars [84], and binary neutron star coalescence [31, 42, 85]. Our adopted rotation law is

$$u^t u_\phi = R_{\rm eq}^2 A^2 (\Omega_c - \Omega) \ , \tag{31}$$

where Ω is the angular velocity of the fluid, Ω_c is the value of Ω on the rotation axis, $R_{\rm eq}$ is the equatorial coordinate radius. The parameter A measures the degree of differential rotation and is chosen to be unity for all cases below, so that the centers of our stars rotate about three times faster than their equators. We take the z-axis to be the rotation axis, and define the cylindrical coordinate radius $\varpi = \sqrt{x^2 + y^2}$. In the Newtonian limit, Eq. (31) reduces to the so-called "j-constant" law [86]

$$\Omega = \frac{\Omega_c}{1 + \frac{\varpi^2}{R_{\rm eq}^2 A^2}} \ . \tag{32}$$

We choose a polytropic index $n = 1$, and take our initial stars to be sufficiently compact so that the collapse does not span a large dynamic range. Accordingly, we are able to use a single, modest grid for each run. As

in [24, 27, 81], we induce collapse by depleting the initial pressure by a factor: $P \to f_P P$. Below, we show results for $f_P = 0.01$. While this form of artificially-induced collapse does not correspond to any realistic astrophysical scenario, there are several situations in which an "effective" pressure depletion does occur. For example, the collapse of the core of a massive star which produces a supernova is brought about by the removal of pressure support both from photo-dissociation of iron-nickel nuclei and the neutronization of the core (de-leptonization). Phase transitions in neutron stars, such as a transition to quark matter, or rapid de-leptonization via neutrino cooling, could also have the effect of inducing pressure depletion. We choose $f_P = 0.01$ to make pressure forces unimportant in comparison with centrifugal forces and gravity. After depleting pressure from the star, we resolve the constraint equations to produce valid initial data. This process of depleting pressure and re-solving the constraints causes M and J to drop by a few percent, while J/M^2 changes by one percent or less.

Table I lists the equilibrium stars used to construct our initial data. These initial data were generated using the code of [76]. Each star has the same rest mass $M_0 = 0.2$, so our stars are members of a sequence uniquely defined by $n = 1$, $A = 1$, $M_0 = 0.2$. This sequence crosses $q = 1$ at one point, between our second and third stars, stars B and C. We expect to find a qualitative difference in the behavior of stars B and C.

Star A is exactly the star studied in the previous section. It is dynamically unstable and collapses without pressure depletion to a Kerr black hole with no disk. Not surprisingly, this is also found to be the behavior when pressure is depleted. We will concentrate below on stars B and C. We begin with simulations in axisymmetry and then discuss simulations in full three dimensions.

A. SubKerr Collapse

Star B has $J/M^2 = 0.9$, so it is subKerr. Its collapse in axisymmetry is shown in Fig. 9. We evolve on a 300^2 grid with outer boundaries at $14M$. At $t = 28.4M$, we locate an apparent horizon with $r_{\rm AH} = 0.62M$, $M_{\rm irr} = 0.72M$. We excise at $t = 29M$, at which time $M_{\rm irr} = 0.74M$, 22% of the rest mass is outside our excision zone, and 15% is outside the apparent horizon. The horizon circumferences at this time are in the ratio $C_{\rm pol}/C_{\rm eq} = 0.76$, which, if this were a stationary Kerr horizon, would correspond to $q = 0.92$. We continue evolving with an excision boundary at radius $r_{\rm ex} = 0.08$. All of the matter falls into the hole within $20M$ after excision is introduced. We evolve for an additional $20M$ after this. We find no signs of numerical instability. Mass conservation is excellent (the amount lost due to gravitational radiation is below 0.1%), but the gradual loss of angular momentum noted in Section IV E is present, as can be seen in Figure 10. We stop evolving when the total angular momentum drops below 80% of its initial value. The final state of the system has, however, been entirely determined well before this time.

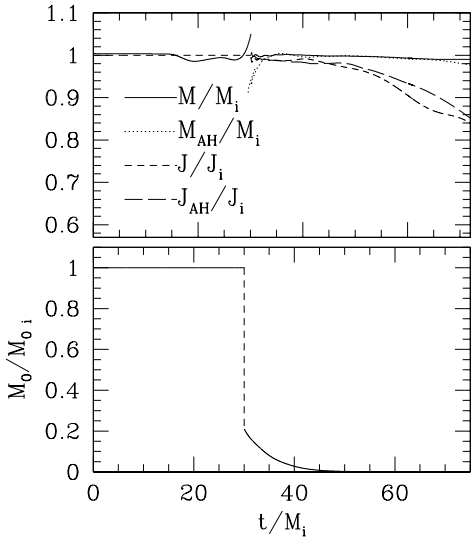

FIG. 10: Diagnostics for the collapse of star B. Above, we show the evolution of M and J calculated from integrations of the exterior spacetime and from measurements of the geometry of the horizon. Below, we plot the total rest mass on the grid, normalized to its initial value. Rest mass is conserved prior to excision. At $t = 30M$, we excise a region from the middle of the grid. This cuts out the matter inside this region, which accounts for 80% of the total rest mass. Over the next $20M$, the remaining rest mass falls into the excision zone, leaving a vacuum being evolved in the outside region.

B. SupraKerr Collapse

Star C has $J/M^2 = 1.2$. We remove the star's pressure support and evolve. In Figure 11, we show the results of a 400^2 axisymmetric run with boundaries at 13 M. With its pressure support removed, the star immediately flattens along the z-axis and moves inward in ϖ. This inward motion toward the axis is halted by centrifugal forces. As seen in the upper right panel of Fig. 11, the inner region of the star stops collapsing before the outer region, so a strong shock is formed. The star then expands into a torus whose radius oscillates with a period close to the initial central rotation period. We show the effects of this oscillation on the maximum rest density and the minimum lapse in Fig. 13. We follow the torus for three oscillations during which time all our constraints are satisfied to better than 10%. The angular momentum J is conserved identically by our no-excision axisymmetric code, but we do find that the ADM mass M decreases gradually with time. This decrease cannot be accounted for by the small flux of rest mass and gravity waves out of the computational domain; the loss therefore represents numerical error. We stop our evolution after three

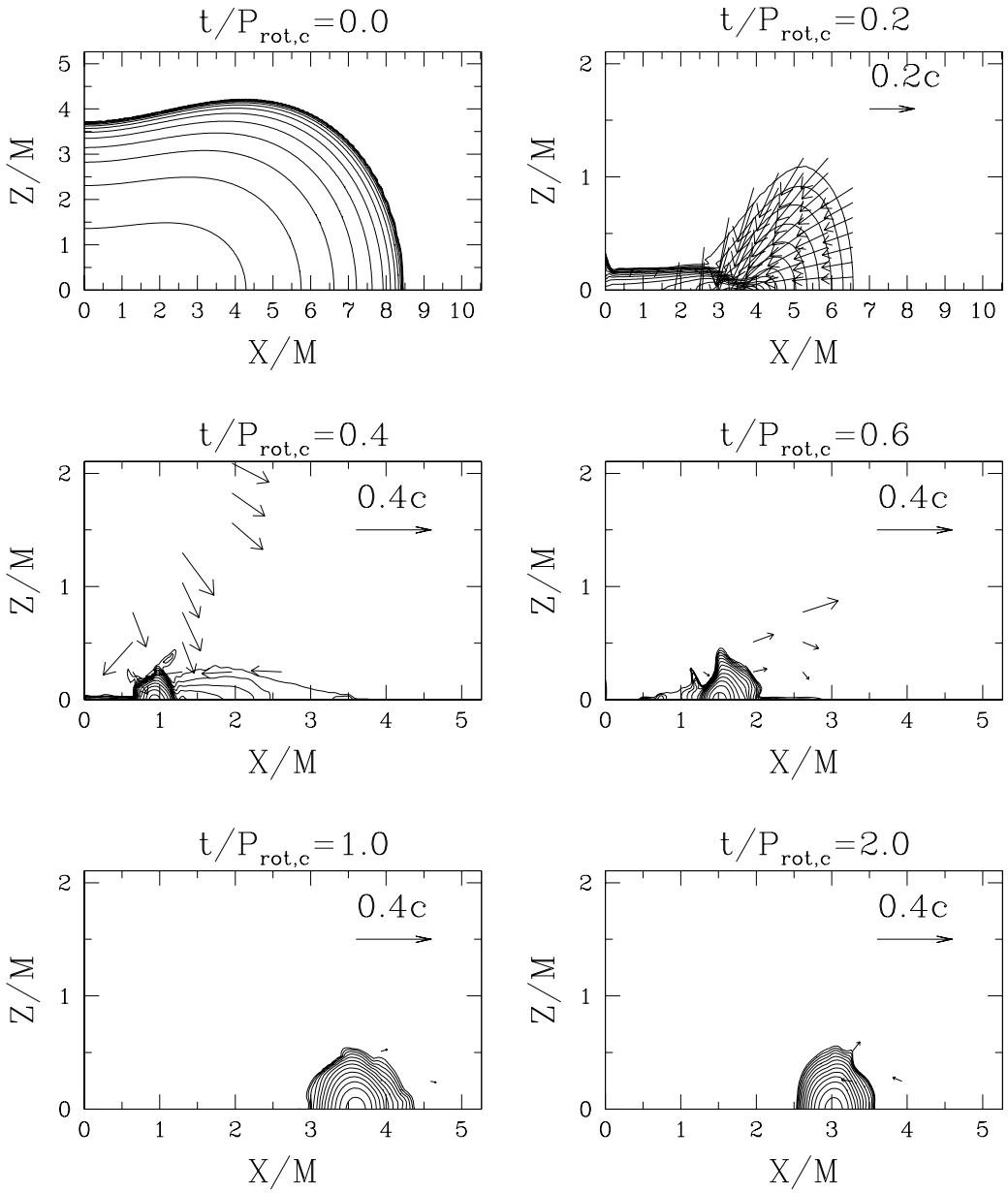

FIG. 11: Snapshots of the rest density contours and the velocity field (v^x, v^z) in the meridional plane during the axisymmetric collapse of star C to a torus. The contours are set as in Figure 9. Some velocity arrows appear outside the contours because the density there is very small but nonzero. Time is normalized to the initial central rotation period of the star, $P_{\rm rot,c} = 98M$.

oscillation periods because M has decreased by ∼15%. To check that the evolution is qualitatively correct, we performed the same run on a 200^2 grid and found that the collapse, torus-formation, and oscillation of the star are very similar at this resolution.

The torus formed in the above simulation could be subject to various non-axisymmetric instabilities. If the rotating torus fragments, the system may produce a large gravitational wave signal ("splash radiation" [51]). It is therefore necessary to perform the above simulation in 3+1 dimensions. We perform this simulation using a $280 \times 140 \times 200$ grid, with boundaries at $[-13M, 13M] \times [0, 13M]^2$, where we use equatorial and π-symmetry. The results are shown in Fig. 12. The collapse, flattening, and formation of the torus occur as in the 2D runs. Then the torus quickly fragments into four clumps symmetrically located about the origin, roughly 90° apart. As these clumps collapse, they ultimately become too small to be evolved accurately on our grid. We conserve M and J to better than 10% throughout the integration shown, and we terminate the calculation when our errors exceed these bounds. To check this result, we have performed

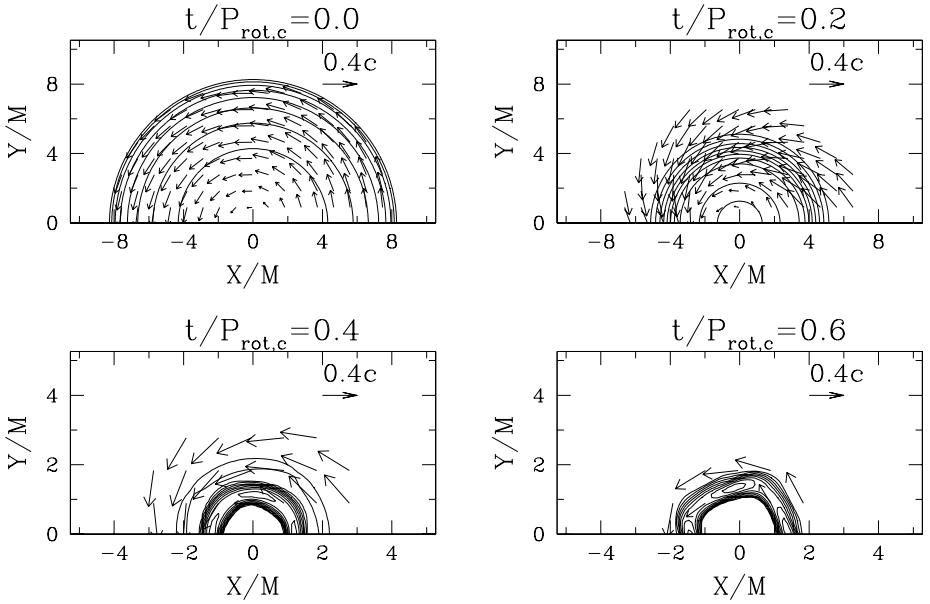

FIG. 12: Snapshots of the rest-density contour lines for ρ_0 and the velocity field (v^x, v^y) in the equatorial plane for the 3D collapse, bounce, and fragmentation of star C. The contours and time normalization are set using the same rule as in Figures 9 and 11. Note that the origin of the system is now shifted to the middle of the x-axis in this plot.

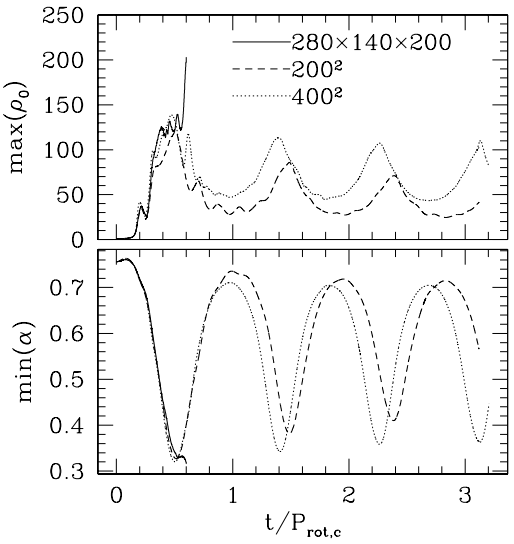

FIG. 13: The maximum value of ρ_0 and the minimum value of α during the evolutions of star C on different grids, plotted as a function of the initial central rotation period $P_{\rm rot,c}$. The two 2D runs are qualitatively similar. The 3D run behaves similarly to the 2D runs for about the first $0.5P_{\rm rot,c}$. Thereafter a nonaxisymmetric instability develops, and the collapsed star fragments.

the same run on $140\times70\times180$ and $100\times50\times100$ grids. In each case, the torus fragments into four pieces 90° apart. In Fig. 13, we compare the behavior of the maximum of ρ_0 and the minimum of α for the evolution of star C in 3D to their behavior in 2D on 200^2 and 400^2 grids.

It has been pointed out by Truelove *et al.* [87] that spurious fragmentation may occur in a numerical simulation if the Jeans length is not well resolved. The Jeans length is given by

$$\lambda_J \sim \sqrt{\frac{\pi c_s^2}{\rho}}\,, \tag{33}$$

where ρ is the density (Mass-energy density and rest-mass density are nearly equal.) and $c_s = \sqrt{\frac{dP}{d\rho}}$ is the sound speed. We can get a lower bound on λ_J by ignoring the large amount of shock heating, which increases c_s, and considering adiabatic compression. Accordingly, for an $n = 1$, $\Gamma = 2$ fluid, $P = \kappa\rho_0^2$, where $\kappa = 0.01$ due to our pressure depletion. Fragmentation occurs when $\rho \approx \rho_0 \approx 3$, so $\lambda_J \sim 0.25 = 15\Delta X$. (Shock heating increases this coefficient.) Our resolution is then quite sufficient to resolve the Jeans length.

We could not determine the final fate of this system. The four clumps may continue to collapse to black holes, or this collapse may be halted by heating-induced pressure. The system will certainly emit substantial amounts of gravity waves, both during the bounce and oscillation of the initially axisymmetric torus and during its rotation following fragmentation. To see this, we measured the gauge invariant Moncrief variables ψ_{lm} (or Zerilli functions) at the outer part of the grid [88]. We also measure the amplitudes of the two gravitational wave polarizations h_+ and $h_\times$ on the x-axis at the edge of our grid.

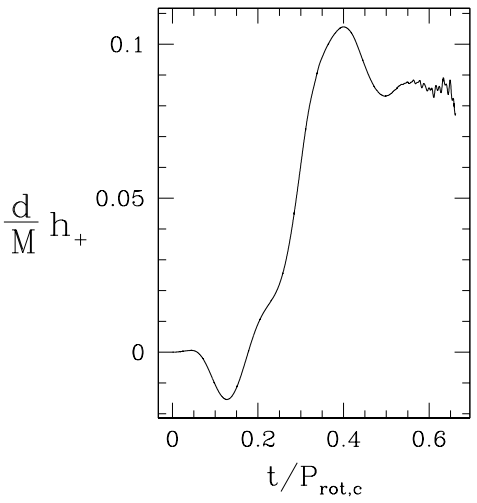

FIG. 14: The gravitational wave amplitude h_+, at a distance d from the source, for the 3D collapse, bounce, and fragmentation of star C. We compute h_+ at the point (11.6 M, 0, 0).

Since the outer part of the grid is not in the wave zone, our measurements are only approximate. We find that the dominant mode of the emission is $l = 2$, $m = 0$, the quadrupole radiation generated by the axisymmetric collapse and bounce of the torus. The second largest modes, which are an order of magnitude smaller than the dominant mode, are $l = 4$, $m = 0$ (octopole radiation from the axisymmetric collapse) and $l = 4$, $m = \pm 4$ (octopole radiation generated by the rotation of the four clumps). In Fig. 14, we plot h_+ on the x-axis, which contains contributions from all modes. The observed amplitude of this radiation from a star at a distance d from the Earth would be

$$h \sim 10^{-22} \left(\frac{M}{M_\odot}\right) \left(\frac{d}{100\mathrm{Mpc}}\right)^{-1} \qquad (34)$$

The final evolution of this very interesting system can only be undertaken using a finer grid, presumably by employing adaptive mesh refinement (AMR), and an improved shock-handling scheme in our code.

VI. DISCUSSION AND CONCLUSIONS

We have constructed a code to study the collapse of astrophysical objects to black holes by evolving the full coupled Einstein-hydrodynamics system in both 2+1 (axisymmetry) and 3+1 dimensions. When a black hole appears, it is treated by introducing an excision boundary well inside the horizon. Our code is stable and convergent for all of the test problems and applications presented here. As a test application, we study the collapse of rapidly rotating stars. Our conclusions regarding their ultimate fate agree with those of Nakamura [79] and of Stark and Piran [81]— namely, that spinning stars deprived of their pressure support will collapse directly to black holes only if they are subKerr. This is the same behavior observed for spinning configurations of collisionless matter [54]. We also were able to study the final state of the subKerr collapses by using our excision algorithm to extend the evolution far beyond what could be achieved without it. We find that even for a rapidly rotating star with $q = 0.9$, all the rest mass falls immediately into the hole, with no disk formation, in agreement with Shibata [28]. For the case of supraKerr collapse, we found that the collapsing star hits a centrifugal barrier and bounces, forming a torus which fragments due to a nonaxisymmetric instability into four pieces. With our current computational resources, we were unable to determine the final fate of the four clumps. Systems like this one are sufficiently interesting as gravitational wave sources, that they should be pursued by further investigation with finer resolution, including AMR.

Considering the stability of our excision algorithm over such a variety of applications, we believe that it has great promise as a tool for relativistic astrophysics involving the simultaneous presence of hydrodynamic matter and black holes. Our current post-excision algorithm exhibits a gradual spurious decrease in total angular momentum when applied at moderate resolution. However, this problem is not present in all coordinate systems (e.g. Kerr-Schild) and is reduced as the resolution is increased. We are currently investigating a number of ways to improve our algorithm and to apply it to other 2D and 3D problems of astrophysical interest.

Acknowledgments

It is a pleasure to thank Charles Gammie, Yuk-Tung Liu, and Branson Stephens for useful discussions. Most of the calculations were performed at the National Center for Supercomputing Applications at the University of Illinois at Urbana-Champaign (UIUC). The remaining calculations were performed at National Center for High-performance Computing in Taiwan. This paper was supported in part by NSF Grants PHY-0090310 and PHY-0205155 and NASA Grant NAG 5-10781.

[1] W.G. Unruh, as cited in J. Thornburg, Class. Quantum Grav. **4**, 1119 (1987).

[2] E. Seidel and W.-M. Suen, Phys. Rev. Lett. **69**, 1845

(1992).
[3] R. L. Marsa and M. W. Choptuik, Phys. Rev. D **54**, 4929 (1996).
[4] P. Anninos *et al*, Phys. Rev. D **51**, 5562 (1995).
[5] R. Gómez, R. L. Marsa, and J. Winicour, Phys. Rev. D **56**, 6310 (1997).
[6] M. A. Scheel, S. L. Shapiro and S. A. Teukolsky, Phys. Rev. D **51**, 4208 (1995); **51**, 4236 (1995)
[7] P. Anninos, K. Camarda, J. Massó, E. Seidel, W.-M. Suen, and J. Towns, Phys. Rev. D **52**, 2059 (1995).
[8] Binary Black Hole Grand Challenge Alliance, Phys. Rev. Lett. **80**, 2512 (1998).
[9] M. Shibata and T. Nakamura, Phys. Rev. D **52**, 5428 (1995).
[10] T. W. Baumgarte and S. L. Shapiro, Phys. Rev. D **59**, 024007 (1999).
[11] M. Alcubierre and B. Brügmann, Phys. Rev. D **63**, 104006 (2001).
[12] H.-J. Yo, T. W. Baumgarte, and S. L. Shapiro, Phys.Rev. D **66**, 084026 (2002).
[13] M. A. Scheel, L. E. Kidder, L. Lindblom, H. P. Pfeiffer, and S. A. Teukolsky, Phys. Rev. D **66**, 124005 (2002).
[14] G. Calabrese *et al*, Class. Quant. Grav. **20** L245 (2003).
[15] M. Tiglio, L. Lehner, and D. Neilsen, gr-qc/0312001 (2003).
[16] R. Gómez, L. Lehner, R. L. Marsa, J. Winicour, Phys. Rev. D **57**, 4778 (1998).
[17] M. Alcubierre, B. Brügmann, D. Pollney, E. Seidel, and R. Takahashi, Phys.Rev. D **f64** 061501 (2001)
[18] D. Shoemaker *et al* Class. Quant. Grav. **20** 3729 (2003).
[19] U. Sperhake *et al*, gr-qc/0307015 (2003).
[20] S. Brandt *et al*, Phys. Rev. Lett. **85**, 5496 (2000).
[21] B. Brügmann, W. Tichy, and N. Jansen, gr-qc/0312112 (2003).
[22] M. Shibata, Phys. Rev. D **60**, 104052 (1999).
[23] J. A. Font, M. Miller, W. M. Suen, and M. Tobias, Phys. Rev. D **61**, 044011 (2000); J. Font *et al*, Phys.Rev. D **65**, 084024 (2002).
[24] M. D. Duez, P. Marronetti, S. L. Shapiro, and T. W. Baumgarte, Phys.Rev. D **67** 024004 (2003).
[25] M. Shibata, T. W. Baumgarte, and S. L. Shapiro, Phys. Rev. D **61**, 044012 (2000).
[26] T. W. Baumgarte, S. L. Shapiro, and M. Shibata, Astrophys. J. **528**, L29 (2000).
[27] M. Shibata, Prog. Theor. Phys. **104** 325 (2000).
[28] M. Shibata, Astrophys.J. **595** 992 (2003).
[29] M. Shibata and S. L. Shapiro, Astrophys. J. **572**, L39 (2002);
[30] P. Marronetti, M. D. Duez, S. L. Shapiro, and T. W. Baumgarte, gr-qc/0312036 (2003).
[31] M. Shibata and K. Uryu, Phys. Rev. D **61**, 064001 (2000); Prog. Theor. Phys. **107** 265 (2002).
[32] M. Shibata, K. Taniguchi, and K. Uryu, gr-qc/0310030 (2003).
[33] C. L. Fryer, Astrophys. J. **522**, 413 (1999).
[34] S. Balberg, L. Zampieri, and S. L. Shapiro, Astrophys. J. **541**, 860 (2000) and references therein.
[35] A. I. MacFadyen and S. E. Woosley, Astrophys. J. **524**, 262 (1999); A. I. MacFadyen, S. E. Woosley, and A. Heger, Astrophys. J. **550**, 410 (2001).
[36] T. J. Galama *et al*, Nature **395**, 670 (1998).
[37] J. S. Bloom, Nature **401**, 453 (1999); A. J. Castro-Tirado and J. Gorosabel, Astron. Astrophys. Suppl. Ser. **138**, 449 (1999); P. Garnavich *et al*, Astrophys. J. **582**, 924 (2003).
[38] J. N. Reeves *et al*, Nature **416**, 512 (2002).
[39] J. Hjorth *et al*, Nature **423** 847 (2003).
[40] T. Piran, Phys. Rep. **314**, 575 (1999); M. H. P. M. van Putten, Phys. Rep. **345**, 1 (2001).
[41] R. Narayan, B. Paczynski, and T. Piran, Astrophys. J. **395**, L83 (1992).
[42] F. A. Rasio, and S. L. Shapiro, Astrophys. J., **401**, 226 (1992); F. A. Rasio, and S. L. Shapiro, Astrophys. J. **432**, 242 (1994); F. A. Rasio, and S. L. Shapiro, Class. Quant. Grav. **16**, R1 (1999).
[43] S. L. Shapiro, Astrophys. J. **544**, 397 (2000); J. N. Cook, S. L. Shapiro, and B. C. Stephens, astro-ph/0310304 (2003); Y. T. Liu and S. L. Shapiro, astro-ph/0312038 (2003).
[44] M. D. Duez, Y. T. Liu, S. L. Shapiro, and B. C. Stephens in preparation.
[45] M. A. Abramowicz, M. Calvani, and L. Nobili, Nature **302**, 597 (1983); S. Nishida, A. Lanza, Y. Eriguchi, and M. A. Abramowicz, Mon. Not. R. Astron. Soc. **278**, L41 (1996); J. A. Font and F. Daigne, Mon. Not. R. Astron. Soc. **334**, 883 (2002); O. Zanotti, L. Rezzolla, and J. A. Font,*ibid.* **341**, 832 (2003).
[46] J. M. Centrella, K. C. B. New, L. L. Lowe, and J. D. Brown, Astrophys. J. **550**, L193 (2001); M. Saijo, T. W. Baumgarte, and S. L. Shapiro, Astrophys. J. **595**, 352 (2002).
[47] S. L. Shapiro, in *The Astrophysics of Gravitational Wave Sources*, ed. J. M. Centrella (Melville, New York, 2003), p. 50.
[48] L. Barack and C. Cutler, gr-qc/0310125 (2003).
[49] M. J. Rees, ARA & A **22**, 471 (1984); T. W. Baumgarte and S. L. Shapiro, Astrophys. J. **526**, 941 (1999); see S. L. Shapiro, to appear in *Carnegie Observatories Astrophysics Series, Vol. 1: Coevolution of Black Holes and Galaxies*, ed. L. C. Ho (Cambridge: Cambridge Univ. Press) for discussion and references.
[50] S. Brandt, J. A. Font, J. M. Ibanez, J. Masso, and E. Seidel, Comput. Phys. Commun. **124**, 169 (2000).
[51] M. Rees, R. Ruffini, and J. A. Wheeler, *Black Holes, Gravitational Waves, and Cosmology: An Introduction to Current Research* (Gordon and Breach, New York, 1974), p. 134.
[52] M. Alcubierre *et al*, Int .J. Mod. Phys. D **10**, 273 (2001).
[53] M. W. Choptuik, E. W. Hirschmann, S. L. Liebling, and F. Pretorius, Class. Quant. Grav. **20**, 1857 (2003).
[54] A. M. Abrahams, G. B. Cook, S. L. Shapiro, and S. A. Teukolsky, Phys. Rev. D **49**, 5153 (1994).
[55] H. O. Kreiss and J. Oliger, *Methods for the Approximate Solution of Time Dependent Problems*, GARP Publication Series No. 10 (World Meteorological Organization, Geneva, 1973).
[56] L. E. Kidder, M. A. Scheel, and S. A. Teukolsky, Phys. Rev. D **64**, 064017 (2001).
[57] S. Detweiler, Phys. Rev. D **35**, 1095 (1987).
[58] G. Yoneda and H. A. Shinkai, Phys. Rev. D **63**, 124019 (2001).
[59] B. Kelly, P. Laguna, K. Lockitch, J. Pullin, E. Schnetter, D. Shoemaker, and M. Tiglio, Phys. Rev. D **64**, 084013 (2001).
[60] G. Yoneda and H. A. Shinkai, Phys. Rev. D **66**, 124003 (2002).
[61] M. Anderson and R. A. Matzner, gr-qc/0307055 (2003).
[62] M. Alcubierre *et al.*, Phys. Rev. D **62**, 044034 (2000).

[63] M. Shibata, Prog. Theor. Phys. **101**, 1199 (1999).
[64] J. A. Font, *Living Rev. in Relativity*, (2003), **6**, http://www.livingreviews.org/lrr-2003-4/.
[65] G. Calabrese and D. Neilsen, gr-qc/0308008 (2003).
[66] M. Alcubierre, Class. Quant. Grav. **20** 607 (2003).
[67] N. Ó. Murchadha and J. W. York Jr., Phys. Rev. D **10**, 2345 (1974); J. M. Bowen and J. W. York, Jr., Phys. Rev. D **21**, 2047 (1980).
[68] T. W. Baumgarte, G. B. Cook, M. A. Scheel, S. L. Shapiro, and S. A. Teukolsky, Phys. Rev. D **54**, 4849 (1996).
[69] S. L. Shapiro and S. A. Teukolsky, *Black Holes, White Dwarfs, and Neutron Stars* (Wiley, New York, 1983), Appendix G.
[70] P. Papadopoulos and J. A. Font, Phys. Rev. D **58**, 024005 (1998).
[71] J. R. Oppenheimer and H. Snyder, Phys. Rev. **56**, 455 (1939)
[72] L.I. Petrich, S.L. Shapiro, and S.A. Teukolsky, Phys. Rev. D **31**, 2459 (1985)
[73] L.I. Petrich, S.L. Shapiro, and S.A. Teukolsky, Phys. Rev. D **33**, 2100 (1986)
[74] J. R. Oppenheimer and G. Volkoff, Phys. Rev. **55**,374 (1939).
[75] See [76] for scaling to arbitrary κ.
[76] G. B. Cook, S. L. Shapiro, and S. A. Teukolsky, Astrophys. J. **398**, 203 (1992).
[77] R. Penrose, Nuovo Cim. **1**, 252 (1969).
[78] T. Nakamura, in *Proceedings of the 12th Workshop on General Relativity and Gravitation in Japan*, edited by M. Shibata *et al* (University of Tokyo, Tokyo, 2002), p. 81.
[79] T. Nakamura, Prog. Theor. Phys. **65**, 1876 (1981).
[80] H. Sato and T. Nakamura, Prog. Theor. Phys. **66**, 2038 (1981).
[81] R. F. Stark and T. Piran, Phys. Rev. Lett. **55**, 891 (1985).
[82] S. L. Shapiro and M. Shibata, Astrophys. J. **577** 904 (2002).
[83] T. Zwerger and E. Müller, Astro. & Astrophys., **320**, 209 (1997).
[84] Y. T. Liu and L. Lindblom, Mon. Not. R. Astron. Soc., **324**, 1063 (2001).
[85] J. A. Faber and F. A. Rasio, Phys.Rev. D **65**, 084042 (2002).
[86] Y. Eriguchi and E. Müller, Astro. & Astrophys., **146**, 260 (1985).
[87] J. K. Truelove *et al*, Astrophys. J. **489**, L179 (1997).
[88] V. Moncrief, Ann. Phys. **88**, 323 (1974).